Three-Dimensional Velocity Field Using the Cross-Model Viscosity Function

Fernando Carapau, Paulo Correia, and Pedro Areias

1 Introduction

Let us consider the constitutive equation for an incompressible and homogeneous linearly viscous fluid where the Cauchy stress tensor is given by

$$\boldsymbol{T} = -p\boldsymbol{I} + 2\mu\boldsymbol{D}, \tag{1}$$

where p is the hydrostatic pressure, μ the constant viscosity, and $\boldsymbol{D}$ the symmetric part of the velocity gradient, also called the rate of deformation tensor

$$\boldsymbol{D} := \frac{1}{2}\Big(\nabla\boldsymbol{\vartheta} + \big(\nabla\boldsymbol{\vartheta}\big)^T\Big), \tag{2}$$

where[1] $\boldsymbol{\vartheta} = \boldsymbol{\vartheta}(\boldsymbol{x}, t)$ is the three-dimensional velocity field, $\nabla\boldsymbol{\vartheta}$ is the spatial velocity gradient, and $\big(\nabla\boldsymbol{\vartheta}\big)^T$ denotes the transpose of $\nabla\boldsymbol{\vartheta}$. The fluids that comply with Eq. (1) are known in the scientific literature as Newtonian fluids. On the other hand, there are fluids for which the viscosity is not constant, and it may depend on

[1] Let $\boldsymbol{x} = (x_1, x_2, x_3)$ be the rectangular space Cartesian coordinates (for convenience, we set $x_3 = z$) and t is the time variable.

F. Carapau (✉) · P. Correia
Departamento de Matemática and CIMA, Universidade de Évora, Évora, Portugal
e-mail: flc@uevora.pt; pcorreia@uevora.pt

P. Areias
Departamento de Engenharia Mecânica, Universidade Técnica de Lisboa, IST, Lisboa, Portugal
e-mail: pedro.areias@tecnico.ulisboa.pt

© The Author(s), under exclusive license to Springer Nature Switzerland AG 2022

F. Carapau, A. Vaidya (eds.), *Recent Advances in Mechanics and Fluid-Structure Interaction with Applications*, Advances in Mathematical Fluid Mechanics,
https://doi.org/10.1007/978-3-031-14324-3_2

certain parameters, as pressure and/or shear rate. These fluids for which the viscosity is not constant are known as non-Newtonian fluids.

For many real fluids, the viscosity of the flow changes with the intensity of the rate of deformation tensor (see, for example, [1]). This change of the viscosity can be very large in some fluids, and it cannot be ignored. Throughout this work, we will consider that the viscosity only depends on the intensity of the shear rate. The simplest way to model such behavior is to introduce in (1) the viscosity as a function of shear rate:

$$\mu(|\dot{\gamma}|) : \mathbb{R}^+ \to \mathbb{R}^+,$$

where $\dot{\gamma}$ is a scalar measure of the rate of shear defined by

$$|\dot{\gamma}| = \sqrt{2\boldsymbol{D} : \boldsymbol{D}}.$$

Therefore, the Cauchy stress tensor in (1) takes the form

$$\boldsymbol{T} = -p\boldsymbol{I} + \mu(|\dot{\gamma}|)\Big(\nabla\boldsymbol{\vartheta} + (\nabla\boldsymbol{\vartheta})^T\Big). \tag{3}$$

The class of non-Newtonian fluids satisfying condition (3) is called generalized Newtonian fluids (or quasi-Newtonian). In general, we can divide the generalized Newtonian fluid into two subclass: the shear-thinning (or pseudoplastic) fluids where the viscosity decreases with the increasing shear rate and the shear-thickening (or dilatant) fluids for which the viscosity increases with the increasing shear rate. The shear-thinning behavior is commonly observed in real fluids, for example, suspensions, emulsions, polymeric fluids (see, for example, [2–4]). The shear-thickening behavior is less common, although it can be observed at highly loaded suspensions, for example, starch, plaster, and a few unusual polymeric fluids (see, for example, [2–4]).

Next, we will present the specific viscosity function under study in this work, that is, the cross model, where the viscosity function in (3) is given by

$$\mu(|\dot{\gamma}|) = \mu_\infty + \frac{\mu_0 - \mu_\infty}{1 + (k|\dot{\gamma}|)^{1-n}}. \tag{4}$$

Here, parameters k and n are called the consistency index and the flow index (positive constants), respectively. In this model, we consider fluids with bounded low μ_0 and high limiting viscosities μ_∞. Considering, $n = 1$ in Eq. (4), the Cauchy stress tensor (3) corresponds to the Newtonian fluid behavior with $\mu = (\mu_\infty + \mu_0)/2$. Moreover, if $n < 1$, we obtain

$$\lim_{|\dot{\gamma}|\to\infty} \mu(|\dot{\gamma}|) = \mu_\infty, \quad \lim_{|\dot{\gamma}|\to 0} \mu(|\dot{\gamma}|) = \mu_0,$$

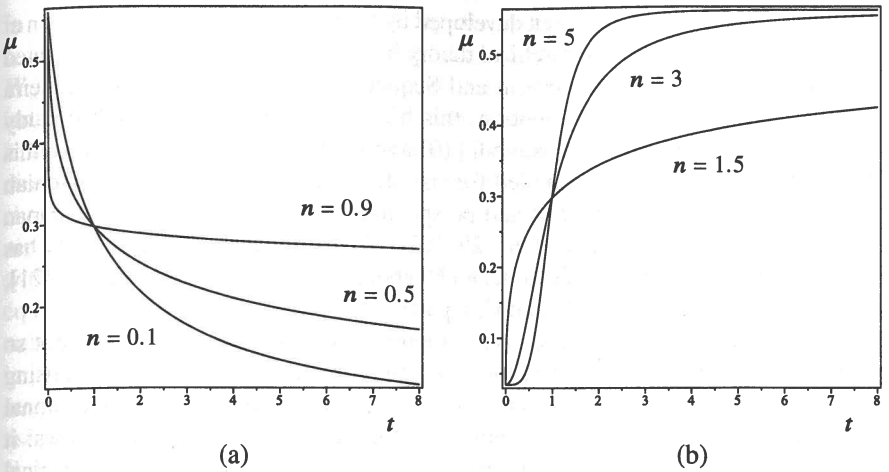

Fig. 1 Cross model: (**a**) shear-thinning viscosity and (**b**) shear-thickening viscosity. Both cases with values $k = 1.007$ s, $\mu_0 = 0.56$ poise, and $\mu_\infty = 0.0345$ poise (see, for example, [5, 6]), for different values of flow index

and the fluid shows us a shear-thinning behavior (see Fig. 1). If $n > 1$, then

$$\lim_{|\dot{\gamma}|\to\infty} \mu(|\dot{\gamma}|) = \mu_0, \quad \lim_{|\dot{\gamma}|\to 0} \mu(|\dot{\gamma}|) = \mu_\infty,$$

and we have a shear-thickening fluid behavior (see Fig. 1).

Numerical simulations relating to a three-dimensional model for a homogeneous incompressible fluid based on the Cauchy stress tensor (3) with viscosity function (4), for a given geometry, require a high computational effort. In this sense, theories that allow us to reduce the complexity of the problems under study by reducing variables are important. A possible simplification is to consider the evolution of average flow quantities using simpler one-dimensional models. Usually, classical one-dimensional models are obtained by imposing additional assumptions related to the nonlinear convective acceleration and the viscous dissipation terms. These closure approximations are typically based on assuming a purely axial flow with a field dependence on axial variables (see, for example, [7–9]). In this work, we present an alternative theory to reduce the three-dimensional model under study to a one-dimensional system of ordinary differential equations, which depend only on time and on a single spatial variable, by using the Cosserat theory associated with fluid dynamics (see Caulk and Naghdi [10]). The basis of this theory (see Duhem [11]) and Eugène and François Cosserat [12]) is to consider an additional structure of deformable vectors (called directors) assigned to each point on a spatial curve (the Cosserat curve). The use of directors in continuum mechanics goes back to Duhem [11], who regarded a body as a collection of points, together with associated directions. This theory has also been used by several authors in studies of rods, plates, and shells (see, for example, [13–17]). An analogous hierarchical theory

related to fluid dynamics has been developed by Caulk and Naghdi [10] and Green et al. [18–20]. Recently, this hierarchical theory has been applied to models associated with hemodynamics (see Robertson and Sequeira [21] and Carapau and Sequeira [22]). Regarding the swirling motion, this hierarchical theory was used to study several models (see Caulk and Naghdi [10] and Carapau et al. [23–25]). Also, this hierarchical theory has been applied for specific models related to non-Newtonian fluids under different geometries and perspectives (see Carapau [26, 27], Carapau and Correia [28], and Carapau et al. [29, 30]). This alternative approach theory has been validated by the works of Caulk and Naghdi [10], Robertson and Sequeira [21], Carapau and Sequeira [22, 29], and Carapau [27].

The advantage of using the Cosserat theory related to fluid dynamics is not so much getting an approximation of the three-dimensional system but rather in using it as an independent framework to predict some properties of the three-dimensional problem under study. The main features of the director theory are as follows: it incorporates all components of the linear momentum equation; it is a hierarchical theory, making it possible to increase the accuracy of the model; the system of equations is closed at each order and therefore unnecessary to make assumptions about the form of the nonlinear and viscous terms; invariance under superposed rigid body motions is satisfied at each order; the wall shear stress enters directly as a dependent variable in the formulation; and the director theory has been shown to be useful for modeling flow in curved tubes, considering many more directors than in the case of a straight tube. A detailed discussion about Cosserat theory, related to fluid dynamics, can be found in [10, 18–20]. The three-dimensional numerical study of the flow associated with an incompressible fluid that follows the constitutive equation (3) with viscosity function (4) in a circular cross-section tube with constant radius is in fact a challenging and complex study in terms of computational effort and infeasible in many relevant issues. Our one-dimensional approach is obtained by integrating the linear momentum equation over the cross section of the tube, taking the three-dimensional velocity field approximation provided by the Cosserat theory. This procedure yields a one-dimensional system, depending only on time and a single spatial variable, which is the axis of the symmetrical flow. This velocity field approximation satisfies exactly both the incompressibility condition and the kinematic boundary condition. Based on the work of Caulk and Naghdi (see [10]), we consider the three-dimensional velocity field $\boldsymbol{\vartheta} = \boldsymbol{\vartheta}(\boldsymbol{x}, t)$ approximated by:[2]

$$\boldsymbol{\vartheta} = \boldsymbol{v} + \sum_{N=1}^{k} x_{\alpha_1} \dots x_{\alpha_N} \boldsymbol{W}_{\alpha_1 \dots \alpha_N}, \tag{5}$$

with

$$\boldsymbol{v} = v_i(z,t)\,\boldsymbol{e}_i, \quad \boldsymbol{W}_{\alpha_1 \dots \alpha_N} = W^i_{\alpha_1 \dots \alpha_N}(z,t)\,\boldsymbol{e}_i. \tag{6}$$

[2] In the sequel, Latin indices take the values 1, 2, and 3 and Greek indices 1 and 2, and we use the convention of summing over repeated indices.

In condition (5), v denotes the velocity along the axis of symmetry z at time t, $x_{\alpha_1} \ldots x_{\alpha_N}$ are the polynomial weighting functions with order k, the vectors $W_{\alpha_1 \ldots \alpha_N}$ are the director velocities which are symmetric with respect to their indices, and e_i are the associated unit basis vectors. We remark that the number k identifies the order in the hierarchical theory and is related to the number of directors. In applications, these director velocities are associated with physical characteristics of the fluid. Considering the velocity field approximation (5) with nine directors (see [10]), i.e., $k = 3$ in (5) and the constitutive condition (3) with viscosity function (4) in our one-dimensional model, we obtain the unsteady equation for mean pressure gradient depending on the volume flow rate, Womersley number, and viscosity parameters over a finite section of a straight, rigid, and impermeable tube with constant circular cross section. Attention is focused on some numerical simulations for constant and nonconstant mean pressure gradient using a Runge-Kutta method. In particular, given a specific data, we get information about the volume flow rate, and consequently we can illustrate the three-dimensional velocity field behavior on the circular cross section of the tube.

2 Governing Equations

Taking into account the constitutive condition (3) with viscosity function (4), we consider the motion of a homogeneous incompressible generalized Newtonian fluid without body forces inside straight rigid and impermeable rectilinear tube with circular cross section of constant radius (see Fig. 2). The boundary of the fluid is defined by the surface scalar constant function ϕ, which is related to the circular cross-section straight tube by the following relationship:

$$\phi^2 = x_1^2 + x_2^2. \tag{7}$$

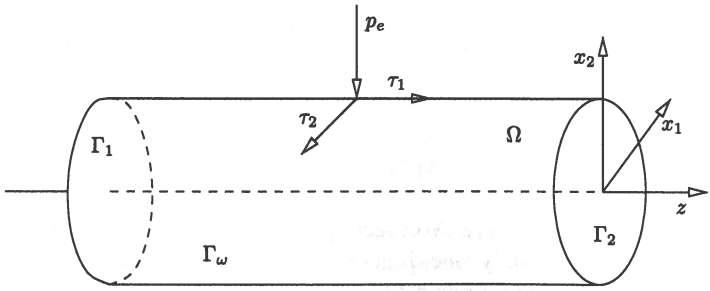

Fig. 2 Fluid domain Ω with normal and tangential components of the surface traction vector p_e and τ_1, τ_2 with constant circular cross section ϕ along the axis of symmetry z. The boundary $\partial\Omega$ is composed by the proximal cross section Γ_1, by the distal cross section Γ_2, and by the lateral wall of the tube Γ_w

Therefore, the equations of motion, considering conservation of linear momentum and mass, are given in $\Omega \times (0, T)$ by

$$\begin{cases} \rho\Big(\dfrac{\partial \boldsymbol{\vartheta}}{\partial t} + \boldsymbol{\vartheta} \cdot \nabla \boldsymbol{\vartheta}\Big) = \nabla \cdot \boldsymbol{T}, \\ \nabla \cdot \boldsymbol{\vartheta} = 0, \\ \boldsymbol{T} = -p\boldsymbol{I} + \Big(\mu_\infty + \dfrac{\mu_0 - \mu_\infty}{1 + (k|\dot{\gamma}|)^{1-n}}\Big)\Big(\nabla \boldsymbol{\vartheta} + (\nabla \boldsymbol{\vartheta})^T\Big), \quad \boldsymbol{t}_w = \boldsymbol{T} \cdot \boldsymbol{n}, \end{cases} \tag{8}$$

with the initial condition

$$\boldsymbol{\vartheta}(\boldsymbol{x}, 0) = \boldsymbol{\vartheta}_0(\boldsymbol{x}) \quad \text{in} \quad \Omega, \tag{9}$$

and the homogeneous Dirichlet boundary condition

$$\boldsymbol{\vartheta}(\boldsymbol{x}, t) = 0 \quad \text{on} \quad \Gamma_w \times (0, T), \tag{10}$$

where ρ is the constant density of fluid. Equation $(8)_1$ represents the balance of linear momentum, and $(8)_2$ is the incompressibility condition. The constitutive equation appears in $(8)_3$ and $\boldsymbol{t}_w$ denotes the stress vector on the surface whose outward unit normal vector is $\boldsymbol{n}(\boldsymbol{x}, t) = n_i(\boldsymbol{x}, t)\boldsymbol{e}_i$. The components of the outward unit normal vector to the surface ϕ are given by

$$n_1 = \frac{x_1}{\phi}, \quad n_2 = \frac{x_2}{\phi}, \quad n_3 = 0. \tag{11}$$

The theoretical study of the model (8)–(10), namely, existence, uniqueness, and regularity of classical and weak solutions, still poses some difficulties. In this work, we are interested in computational simulations of the model (8)–(10), using the director approach related to fluid dynamics. Since Eq. (7) defines a material surface, the three-dimensional velocity field $\boldsymbol{\vartheta}$ must satisfy the kinematic condition[3]

$$\frac{d}{dt}\big(\phi^2 - x_1^2 - x_2^2\big) = 0,$$

i.e.,

$$-x_1\vartheta_1 - x_2\vartheta_2 = 0, \tag{12}$$

on the boundary defined by (7). Averaged quantities such as volume flow rate and pressure are needed to study one-dimensional models. Consider $S = S(z, t)$ a generic axial section of the domain Ω at time t defined by the spatial variable z, bounded by the circle defined by (7), and let $A(z, t)$ be the area of this section $S(z, t)$. Then, the volume flow rate Q is defined by

[3] The material time derivative is given by $\frac{d}{dt}(\,\cdot\,) = \frac{\partial}{\partial t}(\,\cdot\,) + \boldsymbol{\vartheta} \cdot \nabla(\,\cdot\,)$.

$$Q(z,t) = \int_{S(z,t)} \vartheta_3(\boldsymbol{x},t)da, \tag{13}$$

and the average pressure $\bar{p}$ by

$$\bar{p}(z,t) = \frac{1}{A(z,t)} \int_{S(z,t)} p(\boldsymbol{x},t)da. \tag{14}$$

Next, considering (5), it follows (see [10]) that the approximation of the three-dimensional velocity field $\boldsymbol{\vartheta} = \vartheta_i(\boldsymbol{x},t)\boldsymbol{e}_i$ using nine directors is given by

$$\begin{aligned}\boldsymbol{\vartheta} = &\Big[x_1(\xi + \sigma(x_1^2 + x_2^2)) - x_2(\omega + \eta(x_1^2 + x_2^2))\Big]\boldsymbol{e}_1 \\ &+ \Big[x_1(\omega + \eta(x_1^2 + x_2^2)) + x_2(\xi + \sigma(x_1^2 + x_2^2))\Big]\boldsymbol{e}_2 \\ &+ \Big[v_3 + \gamma(x_1^2 + x_2^2)\Big]\boldsymbol{e}_3,\end{aligned} \tag{15}$$

where $\xi, \omega, \gamma, \sigma, and \eta$ are scalar functions of the spatial variable z and time t. The physical significance of these scalar functions in (15) is the following: γ is related to transverse shearing motion, ω and η are related to rotational motion (also called swirling motion) about $\boldsymbol{e}_3$, while ξ and σ are related to transverse elongation. We use nine directors because it is the minimum number for which the incompressibility condition and the kinematic boundary conditions on the lateral surface of the tube are satisfied pointwise. Using the velocity approach (15), the kinematic conditions (12) on the lateral boundary reduce to

$$-\phi^2(\xi + \phi^2\sigma) = 0, \tag{16}$$

and the incompressibility condition given by Eq. $(8)_2$ becomes

$$(v_3)_z + 2\xi + (x_1^2 + x_2^2)(\gamma_z + 4\sigma) = 0, \tag{17}$$

where the subscripted variable denotes partial differentiation. For Eq. (17) to hold at every point in the fluid, the velocity coefficients must satisfy the separate conditions:

$$(v_3)_z + 2\xi = 0, \quad \gamma_z + 4\sigma = 0. \tag{18}$$

Hence, the boundary condition (12) and the incompressibility condition given by Eq. $(8)_2$ are satisfied exactly by the velocity field (15) if we impose the conditions (16) and (18). On the wall boundary of the rigid tube, we impose the no-slip boundary condition requiring that the velocity field (15) vanishes identically on the surface (7), i.e., condition (10) is satisfied. Thus, it follows that

$$\xi + \phi^2\sigma = 0, \quad \omega + \phi^2\eta = 0, \quad v_3 + \phi^2\gamma = 0. \tag{19}$$

Therefore, Eq. (16) is satisfied identically, and the two incompressibility conditions (18) reduce to

$$(v_3)_z + 2\xi = 0, \quad (\phi^2 v_3)_z = 0. \tag{20}$$

Considering the flow in a rigid tube with constant circular cross section given by surface (7) without swirling motion (i.e., $\omega = \eta = 0$), conditions (13), (15), (19), and (20), then the volume flow rate Q is just a function of time t, given by

$$Q(t) = \frac{\pi}{2}\,\phi^2 v_3(z,t), \tag{21}$$

and, consequently, the velocity field (15) can be rewritten as

$$\boldsymbol{\vartheta}(\boldsymbol{x},t) = \frac{2Q(t)}{\pi\phi^2}\Big(1 - \frac{x_1^2 + x_2^2}{\phi^2}\Big)\boldsymbol{e}_3, \tag{22}$$

and the initial condition (9) is satisfied when we consider in computational simulations $Q(0) = \text{const}$.

To simplify the computational effort, it is convenient to introduce the stress vector $\boldsymbol{t}_w$ on the lateral surface in terms of its outward unit normal $\boldsymbol{n}$ and in terms of the components of the surface traction vector τ_1, τ_2 and p_e in the form (see [10])

$$\boldsymbol{t}_w = \tau_1\boldsymbol{\lambda} - p_e\boldsymbol{n} + \tau_2\boldsymbol{e}_\theta, \tag{23}$$

where τ_1 is the wall shear stress, while $\boldsymbol{\lambda}$ and $\boldsymbol{e}_\theta$ are the unit tangent vectors defined by

$$\boldsymbol{\lambda} = \boldsymbol{n} \times \boldsymbol{e}_\theta, \quad \boldsymbol{e}_\theta = (x_\alpha/\phi)\boldsymbol{e}_{\alpha\beta}\boldsymbol{e}_\beta, \tag{24}$$

with $\boldsymbol{e}_{11} = \boldsymbol{e}_{22} = 0$ and $\boldsymbol{e}_{12} = -\boldsymbol{e}_{21} = 1$. Using conditions (11) and (24), the expression for the stress vector (23) can be rewritten in terms of its rectangular Cartesian components as

$$\boldsymbol{t}_w = \frac{1}{\phi}(-p_e x_1 - \tau_2 x_2)\boldsymbol{e}_1 + \frac{1}{\phi}(-p_e x_2 + \tau_2 x_1)\boldsymbol{e}_2 + \tau_1\boldsymbol{e}_3. \tag{25}$$

Next, instead of the momentum equation $(8)_1$ be verified pointwise in the fluid, we impose the following integral conditions (see [10]):

$$\int_S \Big[\nabla\cdot\boldsymbol{T} - \rho\Big(\frac{\partial\boldsymbol{\vartheta}}{\partial t} + \boldsymbol{\vartheta}\cdot\nabla\boldsymbol{\vartheta}\Big)\Big]da = 0, \tag{26}$$

$$\int_S \Big[\nabla\cdot\boldsymbol{T} - \rho\Big(\frac{\partial\boldsymbol{\vartheta}}{\partial t} + \boldsymbol{\vartheta}\cdot\nabla\boldsymbol{\vartheta}\Big)\Big]x_{\alpha_1}\ldots x_{\alpha_N}da = 0, \tag{27}$$

where $N = 1, 2, 3$. Using the divergence theorem and a form of Leibniz rule, Eqs. (26) and (27) for nine directors can be reduced to the following vector equations:

$$\frac{\partial \boldsymbol{h}}{\partial z} + \boldsymbol{f} = \boldsymbol{a}, \tag{28}$$

and

$$\frac{\partial \boldsymbol{m}^{\alpha_1 \ldots \alpha_N}}{\partial z} + \boldsymbol{l}^{\alpha_1 \ldots \alpha_N} = \boldsymbol{k}^{\alpha_1 \ldots \alpha_N} + \boldsymbol{b}^{\alpha_1 \ldots \alpha_N}, \tag{29}$$

where $\boldsymbol{h}$, $\boldsymbol{k}^{\alpha_1 \ldots \alpha_N}$, $\boldsymbol{m}^{\alpha_1 \ldots \alpha_N}$ are resultant forces defined by

$$\boldsymbol{h} = \int_S \boldsymbol{T}_3 da, \quad \boldsymbol{k}^{\alpha} = \int_S \boldsymbol{T}_{\alpha} da, \quad \boldsymbol{k}^{\alpha\beta} = \int_S \Big(\boldsymbol{T}_{\alpha} x_{\beta} + \boldsymbol{T}_{\beta} x_{\alpha}\Big) da, \tag{30}$$

$$\boldsymbol{k}^{\alpha\beta\gamma} = \int_S \Big(\boldsymbol{T}_{\alpha} x_{\beta} x_{\gamma} + \boldsymbol{T}_{\beta} x_{\alpha} x_{\gamma} + \boldsymbol{T}_{\gamma} x_{\alpha} x_{\beta}\Big) da, \tag{31}$$

and

$$\boldsymbol{m}^{\alpha_1 \ldots \alpha_N} = \int_S \boldsymbol{T}_3 x_{\alpha_1} \ldots x_{\alpha_N} da. \tag{32}$$

The quantities $\boldsymbol{a}$ and $\boldsymbol{b}^{\alpha_1 \ldots \alpha_N}$ are inertia terms defined by

$$\boldsymbol{a} = \int_S \rho\Big(\frac{\partial \boldsymbol{\vartheta}}{\partial t} + \boldsymbol{\vartheta} \cdot \nabla \boldsymbol{\vartheta}\Big) da, \tag{33}$$

$$\boldsymbol{b}^{\alpha_1 \ldots \alpha_N} = \int_S \rho\Big(\frac{\partial \boldsymbol{\vartheta}}{\partial t} + \boldsymbol{\vartheta} \cdot \nabla \boldsymbol{\vartheta}\Big) x_{\alpha_1} \ldots x_{\alpha_N} da, \tag{34}$$

and $\boldsymbol{f}$, $\boldsymbol{l}^{\alpha_1 \ldots \alpha_N}$, which arise due to surface traction on the lateral boundary, are defined by

$$\boldsymbol{f} = \int_{\partial S} \boldsymbol{t}_w \, ds, \tag{35}$$

$$\boldsymbol{l}^{\alpha_1 \ldots \alpha_N} = \int_{\partial S} \boldsymbol{t}_w \, x_{\alpha_1} \ldots x_{\alpha_N} ds. \tag{36}$$

Next, we will derive the equation for the mean pressure gradient using the computed values for the quantities (30)–(36) in Eqs. (28)–(29) according to [10].

3 Main Results and Simulations

The computational effort to calculate the quantities (30)–(36) related to the constitutive equation $(8)_3$ for any index flow n (i.e., shear-thinning viscosity and shear-thickening viscosity) is difficult to handle. This difficulty is related to computational problems arising from the calculation of integrals with singularities. However, for some positive integer values of n, the difficulty can be overcome. Therefore, considering the choice $n = 3$ on Eq. $(8)_3$, the equation for the mean pressure gradient will be obtained using the resulting quantities from (30) to (36) on Eqs. (28)–(29).

In sequence, using the velocity field (22), the surface (7), the volume flow rate (21), and the stress vector (25) in Eqs. (30)–(36), we can explicitly calculate the forces $\boldsymbol{h}$, $\boldsymbol{k}^{\alpha}$, $\boldsymbol{k}^{\alpha\beta}$, $\boldsymbol{k}^{\alpha\beta\gamma}$, $\boldsymbol{m}^{\alpha_1\ldots\alpha_N}$, the inertia terms $\boldsymbol{a}$, $\boldsymbol{b}^{\alpha_1\ldots\alpha_N}$, and the surface tractions $\boldsymbol{f}$, $\boldsymbol{l}^{\alpha_1\ldots\alpha_N}$. Hence, plugging these solutions into Eqs. (28)–(29) and using Eq. (14), by solving a linear system, we get the unsteady equation for the average pressure gradient, given by

$$\begin{aligned}\bar{p}_z(z,t) = &-\frac{4\rho}{3\pi\phi^2}Q_t(t) - \frac{8\mu_0}{\pi\phi^4}Q(t)\\ &+ (\mu_0-\mu_\infty)\Big[\frac{\pi^3\phi^8}{64\,k^4\,Q^3(t)}ln\Big(\frac{32k^2Q^2(t)+\pi^2\phi^6}{\pi^2\phi^6}\Big)\\ &- \frac{\pi\phi^2}{2\,k^2\,Q(t)}\Big],\end{aligned} \tag{37}$$

Integrating condition (37) over a finite section of the tube between z_1 and z_2 with $z_1 < z_2$, we obtain the mean pressure gradient over the interval $[z_1, z_2]$ at time t, given by

$$\begin{aligned}G(t) = &\frac{4\rho}{3\pi\phi^2}Q_t(t) + \frac{8\mu_0}{\pi\phi^4}Q(t) + (\mu_0-\mu_\infty)\Big[\frac{\pi\phi^2}{2\,k^2\,Q(t)}\\ &- \frac{\pi^3\phi^8}{64\,k^4\,Q^3(t)}ln\Big(\frac{32k^2Q^2(t)+\pi^2\phi^6}{\pi^2\phi^6}\Big)\Big],\end{aligned} \tag{38}$$

where

$$G(t) = \frac{\bar{p}(z_1,t) - \bar{p}(z_2,t)}{z_2 - z_1}.$$

Next, let us consider the following dimensionless variables:

$$\hat{t} = \omega_0 t, \quad \hat{Q}(\hat{t}) = \frac{2\rho}{\pi\phi k}Q(t), \quad \hat{G}(\hat{t}) = \frac{\rho^3\phi^7}{k^4}G(t), \tag{39}$$

where ω_0 is the characteristic frequency for unsteady flows. In the cases where a steady volume flow rate is specified, the nondimensional volume flow rate $\hat{Q}$ is identical to the classical Reynolds number used for flow in tubes (see Robertson and Sequeira [21]). Substituting the new variables (39) in Eq. (38), we obtain the nondimensional mean pressure gradient:

$$\hat{G}(\hat{t}) = \frac{2}{3}\mathcal{W}_o^2\hat{Q}_{\hat{t}}(\hat{t}) + 4\mathcal{A}_\mu\hat{Q}(\hat{t}) + \mathcal{B}_\mu\Big[\frac{1}{\hat{Q}(\hat{t})} - \frac{1}{8}\frac{C_\mu}{\hat{Q}^3(\hat{t})}ln\Big(8\frac{\hat{Q}^2(\hat{t})}{C_\mu} + 1\Big)\Big], \tag{40}$$

where $\mathcal{W}_o = \phi^3\sqrt{\rho^3\omega_0/k^3}$ is the Womersley number, which is the most commonly used parameter to reflect the pulsatility of the flow and $\mathcal{A}_\mu$, $\mathcal{B}_\mu$, and C_μ are viscosity parameters, given by

$$\mathcal{A}_\mu = \frac{\mu_0\rho^2\phi^4}{k^3},\ \mathcal{B}_\mu = \frac{(\mu_0 - \mu_\infty)\rho^4\phi^4}{k^7},\ C_\mu = \frac{\rho^2\phi^4}{k^4}. \tag{41}$$

Moreover, using $(39)_2$ and the dimensionless variables

$$\hat{x}_1 = \frac{x_1}{\phi},\quad \hat{x}_2 = \frac{x_2}{\phi},\quad \hat{z} = \frac{z}{\phi},\quad \hat{\boldsymbol{v}}(\hat{\boldsymbol{x}},\hat{t}) = \frac{\phi\rho}{k}\boldsymbol{v}(\boldsymbol{x},t), \tag{42}$$

at the velocity equation (22), we get the nondimensional three-dimensional velocity field:

$$\hat{\boldsymbol{v}}(\hat{\boldsymbol{x}},\hat{t}) = \hat{Q}(\hat{t})\Big(1 - (\hat{x}_1^2 + \hat{x}_2^2)\Big)\boldsymbol{e}_3. \tag{43}$$

In the next section, we present numerical simulations associated with the Eqs. (40) and (43) for specific flow regimes, considering

$$\mathcal{A}_\mu \to 1,\quad \mathcal{B}_\mu \to 0,\quad C_\mu \neq 0, \tag{44}$$

in order to reduce the computational effort.

3.1 *Constant Mean Pressure Gradient*

In Fig. 3, we can observe the behavior of the unsteady volume flow rate solution given by (40) obtained using a Runge-Kutta method with constant mean pressure gradient $\hat{G}(\hat{t}) = 1$ when we increase the Womersley number. Therefore, we note that the amplitude of the solution in the initial transient phase increases and becomes less pronounced as the Womersley number increases. In this particular case of a constant mean pressure gradient, the volume flow rate given by (40)

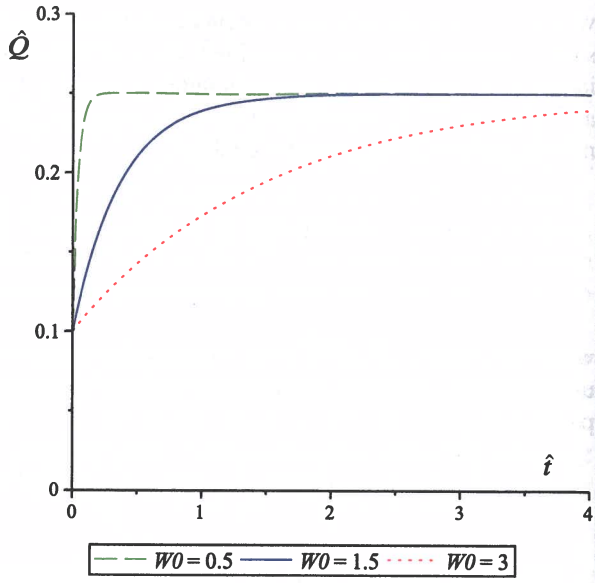

Fig. 3 Unsteady volume flow rate given by Eq. (40) with constant mean pressure gradient $\hat{G}(\hat{t}) = 1$ where $\hat{Q}(0) = 0.1$ and $\mathcal{W}_o = (0.5; 1.5; 3)$ for shear-thickening fluids with $n = 3$

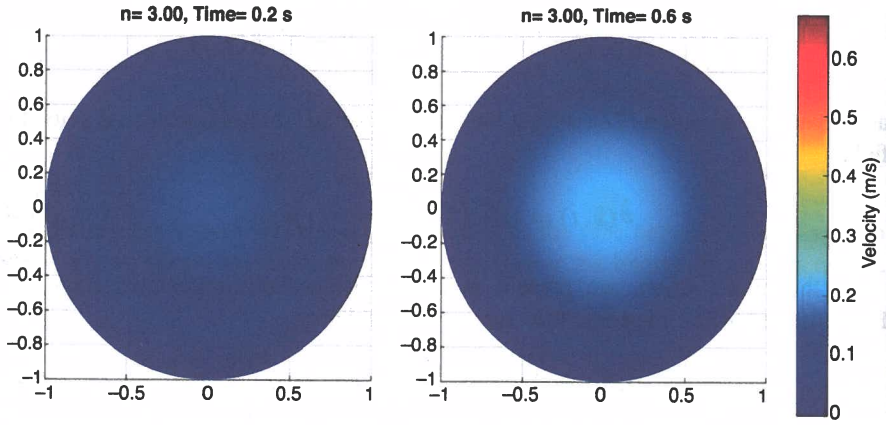

Fig. 4 Three-dimensional velocity field (43) where the volume flow rate is obtained by (40) with $\hat{G}(\hat{t}) = 1$, $\hat{Q}(0) = 0.1$, $\mathcal{W}_o = 1.5$, and $n = 3$ (shear-thickening fluid). Time parameters: $\hat{t} = 0.2$, $\hat{t} = 0.6$

converges toward to the steady-state solution, converging faster for small values of the Womersley number, i.e., when $\mathcal{W}_o \to 0$.

Moreover, with the information of the volume flow rate given by (40), obtained for certain flow regimes, we can return to the three-dimensional problem to obtain the behavior of the three-dimensional velocity field (43) in time on the circular cross section of the tube. Figures 4 and 5 illustrate the three-dimensional velocity field (43) behavior in the circular cross section of the tube when we increase the time parameters.

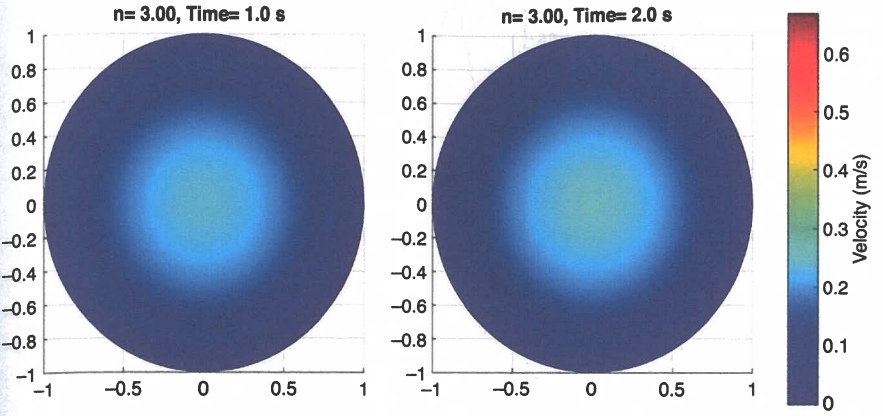

Fig. 5 Three-dimensional velocity field (43) where the volume flow rate is obtained by (40) with $\hat{G}(\hat{t}) = 1$, $\hat{Q}(0) = 0.1$, $\mathcal{W}_o = 1.5$, and $n = 3$ (shear-thickening fluid). Time parameters: $\hat{t} = 1, \hat{t} = 2$

3.2 *Nonconstant Mean Pressure Gradient*

Let us consider the nonconstant mean pressure gradient function, given by

$$\hat{G}(\hat{t}) = 1 + \frac{\sin^2(\hat{t})}{e^{\hat{t}}}, \tag{45}$$

which shows an interesting behavior (see Fig. 6). More specifically, it shows a strong variation in the initial stage and after the initial transient phase has small fluctuations, which tend to decrease with time. In Fig. 7, we can observe the behavior of the unsteady volume flow rate solution given by (40) obtained using a Runge-Kutta method with nonconstant mean pressure gradient (45), when we increase the Womersley number $\mathcal{W}_o = (0.5; 1.5; 3)$. In the initial phase of transition, we can verify the variation of the volume flow rate with the increase of the Womersley number, but with time the volume flow rate tends to stabilize regardless of the period of variation of the nondimensional parameter.

Finally, with the information of the volume flow rate given by (40), obtained for certain flow regimes with nonconstant pressure gradient (45), we can return to the three-dimensional problem to obtain the behavior of the three-dimensional velocity field (43) in time on the circular cross section of the tube (see Figs. 8 and 9).

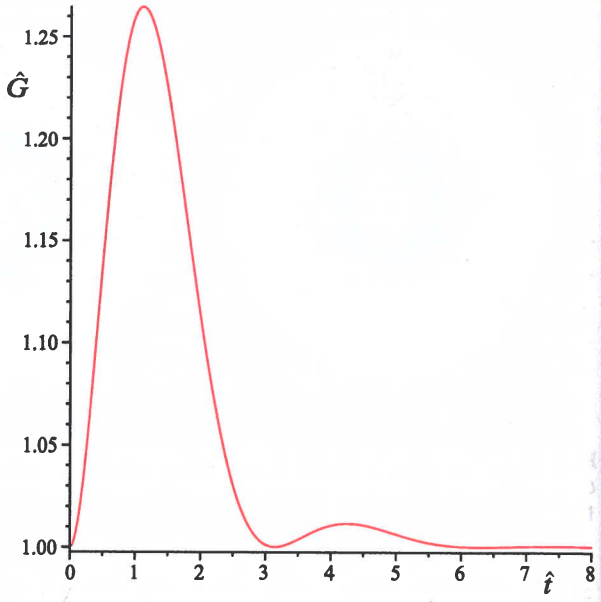

Fig. 6 Nonconstant mean pressure gradient given by Eq. (45)

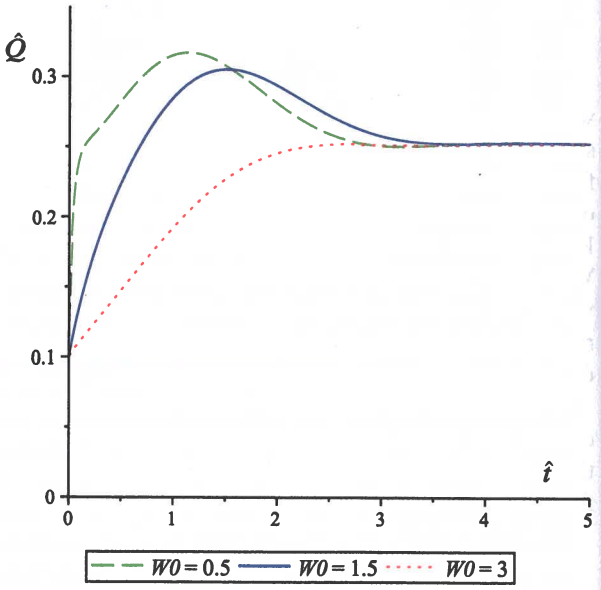

Fig. 7 Unsteady volume flow rate given by Eq. (40) with nonconstant mean pressure gradient (45) where $\hat{Q}(0) = 0.1$ and $\mathcal{W}_o = (0.5; 1.5; 3)$ for shear-thickening fluids with $n = 3$

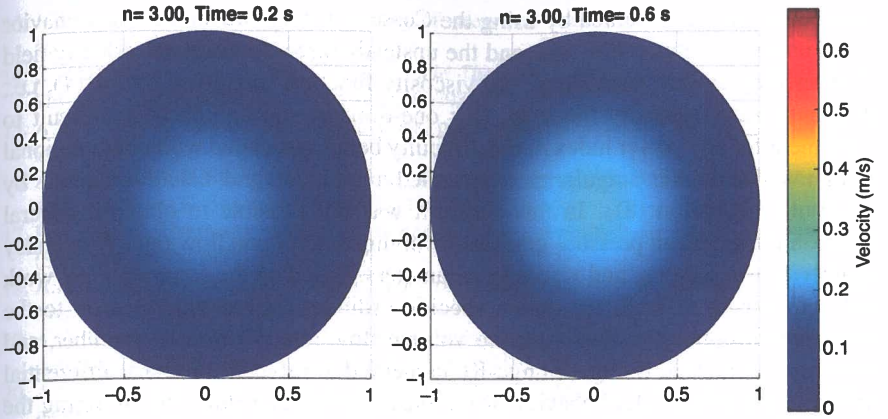

Fig. 8 Three-dimensional velocity field (43) where the volume flow rate is obtained by (40) with nonconstant mean pressure gradient (45), $\hat{Q}(0) = 0.1$, $\mathcal{W}_o = 0.5$, and $n = 3$ (shear-thickening fluid). Time parameters: $\hat{t} = 0.2$, $\hat{t} = 0.6$

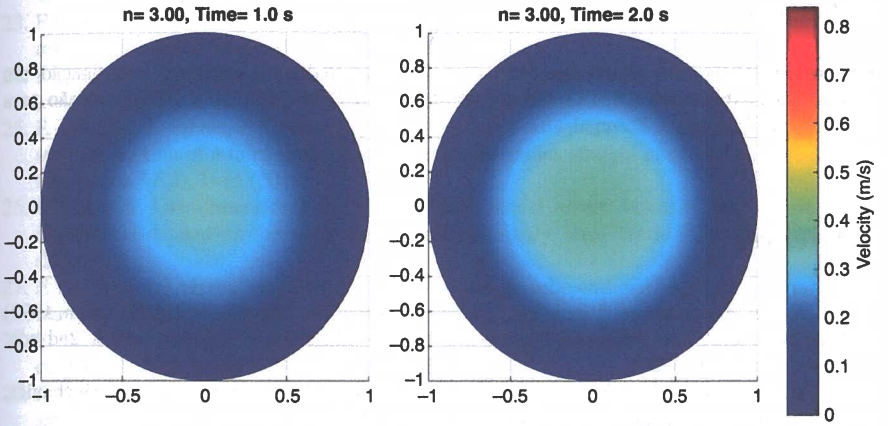

Fig. 9 Three-dimensional velocity field (43) where the volume flow rate is obtained by (40) with nonconstant mean pressure gradient (45), $\hat{Q}(0) = 0.1$, $\mathcal{W}_o = 0.5$, and $n = 3$ (shear-thickening fluid). Time parameters: $\hat{t} = 1$, $\hat{t} = 2$

4 Conclusions

Based on the works [10, 21, 22, 27, 29], we are facing a one-dimensional theory relevant to the study of physical problems involving the flow of Newtonian and non-Newtonian fluids under different geometries and perspectives, being a valid alternative to the classics one-dimensional models. The nature of Eq. (40) shows us in general the difficulty and the challenge of studying the flow of an incompressible fluid where the viscosity varies with the shear rate. In this work, based on a one-

dimensional model obtained by using the Cosserat theory, we studied the behavior of the unsteady volume flow rate and the unsteady three-dimensional velocity field of an incompressible fluid where the viscosity function was given by Eq. (4), i.e., by cross-model viscosity function. Our one-dimensional approach is difficult to implement for any power index n, the difficulty being associated with computational problems due to the singularities presented in the integral calculus caused by constitutive equation $(8)_3$. In this sense, it was not possible to obtain a general equation for the mean pressure gradient involving the volume flow rate, Womersley number, power index n, and viscosity parameters. Based on the computational work and considering $n = 3$, we obtain specific ordinary differential equation to the mean pressure gradient involving the volume flow rate, Womersley number, and viscosity parameters. Using a Runge-Kutta method to solve the ordinary differential equation, we present the behavior of the unsteady volume flow rate by fixing the mean pressure gradient for specific flow regimes. Furthermore, we illustrate the three-dimensional velocity field behavior related to the model (8)–(10). Future work related to the Cosserat theory, which we are currently under study, include fluid-structure interaction, curved tubes, and the case of tubes with branches or bifurcations.

Acknowledgments This work has been partially supported by Centro de Investigação em Matemática e Aplicações (CIMA), through the grant UIDB/04674/2020 of FCT-Fundação para a Ciência e a Tecnologia, Portugal.

References

1. S.L. Rosen, *Fundamental Principles of Polymeric Materials*, 2nd edn. (Wiley, Hoboken, 1993)
2. B.R. Bird, R.C. Armstrong, O. Hassager, *Dynamics of Polymeric Liquids*, vol. 1, 2nd edn. (Wiley, Hoboken, 1987)
3. N.P. Cheremisinoff, *Rheology and Non-Newtonian Flows*. Encyclopedia of Fluid Mechanics, ed. by N.P. Cheremisinoff , vol. 7 (Springer, Berlin, 1986)
4. E. Marušić-Paloka, Steady flow of a non-newtonian fluid in unbounded channels and pipes. Math. Models Methods Appl. Sci. **10**(9), 1425–1445 (2000)
5. Y.I. Cho, K.R. Kensey, Effects of non-newtonian viscosity of blood on flows in a diseased arterial vessel, part 1: steady flows. Biorheology **28**, 41–262 (1991)
6. K.K. Yeleswarapu, Evaluation of continuum models for characterizing the constitutive behavior of blood. Ph.D. Thesis, University of Pittsburgh, 1996
7. T. Huges, J. Lubliner, On the one-dimensional theory of blood flow in the larger vessels, Math. Biosci. **18**, 161–170 (1973)
8. S.J. Sherwin, V. Franke, J. Peiró, K. Parker, One-dimensional modelling of a vascular network in space-time variables. J. Eng. Math. **47**, 217–250 (2003)
9. L. Formaggia, D. Lampont, A. Quarteroni, One-dimensional models for blood flow in arteries. J. Eng. Math. **47**, 251–276 (2003)
10. D. Caulk, P.M. Naghdi, Axisymmetric motion of viscous fluid flow inside a slender surface of revolution. J. Appl. Mech. **54**, 190–196 (1987)
11. P. Duhem, Le potentiel thermodynamique et la pression hydrostatique. Ann. École Norm **10**, 187–230 (1893)
12. E. Cosserat, F. Cosserat, Sur la théorie des corps minces. Compt. Rend. **146**, 169–172 (1908)

13. J.L. Ericksen, C. Truesdell, Exact theory of stress and strain in rods and shells. Arch. Rat. Mech. Anal. **1**(1), 295–323 (1958)
14. C. Truesdell, R. Toupin, *The Classical Field Theories of Mechanics*, ed. by Handbuch der Physik III (Springer, Berlin, 1960), pp. 226–793
15. A.E. Green, N. Laws, P.M. Naghdi, Rods, plates and shells. Proc. Camb. Phil. Soc. **64**(1), 895–913 (1968)
16. A.E. Green, P.M. Naghdi, M.L. Wenner, On the theory of rods II. Developments by direct approach. Proc. R. Soc. Lond. A **337**(1), 485–507 (1974)
17. P.M. Naghdi, The theory of shells and plates, in *Flügg's Handbuch der Physik*, vol. VIa/2, edn. (Springer, Berlin, 1972), pp. 425–640
18. A.E. Green, P.M. Naghdi, A direct theory of viscous fluid flow in channels. Arch. Ration. Mech. Analy. **86**, 39–63 (1984)
19. A.E. Green, P.M. Naghdi, A direct theory of viscous fluid flow in pipes I: basic general developments. Phil. Trans. R. Soc. Lond. A **342**(1), 525–542 (1993)
20. A.E. Green, P.M. Naghdi, A direct theory of viscous fluid flow in pipes: II flow of incompressible viscous fluid in curved pipes. Phil. Trans. R. Soc. Lond. A **342**(1), 543–572 (1993)
21. A.M. Robertson, A. Sequeira, A director theory approach for modeling blood flow in the arterial system: an alternative to classical 1D models. Math. Models Methods Appl. Sci. **15**(6), 871–906 (2005)
22. F. Carapau, A. Sequeira, 1D models for blood flow in small vessels using the cosserat theory. WSEAS Trans. Math. **5**(1), 54–62 (2006)
23. F. Carapau, Axisymmetric swirling motion of viscoelastic fluid flow inside a slender surface of revolution. IAENG Eng. Lett. **17**(4), 238–245 (2009)
24. F. Carapau, J. Janela, A one-dimensional model for unsteady axisymmetric swirling motion of a viscous fluid in a variable radius straight circular tube. Int. J. Eng. Sci. **72**, 107–116 (2013)
25. F. Carapau, J. Janela, P. Correia, S. Vila, Numerical solvability of a cosserat model for the swirling motion of a third-grade fluid in a constant radius straight circular tube. Int. J. Appl. Math. Stat. **57**(2), 1–15 (2018)
26. F. Carapau, One-dimensional viscoelastic fluid model where viscosity and normal stress coefficients depend on the shear rate. Nonlinear Analy. Real World Appl. **11**, 4342–4354 (2010)
27. F. Carapau, 1D viscoelastic flow in a circular straight tube with variable radius. Int. J. Appl. Math. Stat., No. D10 **19**, 20–39 (2010)
28. F. Carapau, P. Correia, Numerical simulations of a third-grade fluid flow on a tube through a contraction. Eur. J. Mech. B/Fluids **65**, 45–53 (2017)
29. F. Carapau, A. Sequeira, Axisymmetric motion of a second order viscous fluid in a circular straight tube under pressure gradients varying exponentially with time. WIT Trans. Eng. Sci. **52**, 409–419 (2006)
30. F. Carapau, P. Correia, T. Rabczuk, P. Areias, One-dimensional model for the unsteady flow of a generalized third-grade viscoelastic fluid. Neural Comput. Appl. **32**(16), 12881–12894 (2020)